

Accepted Manuscript

Synthesis and *in vitro* phototoxicity of multifunctional Zn(II)meso-tetrakis(4-carboxyphenyl)porphyrin-coated gold nanoparticles assembled *via* axial coordination with imidazole ligands

María E. Alea-Reyes, Oriol Penon, Paula García Calavia, María J. Marín, David A. Russell, Lluïsa Pérez-García

PII: S0021-9797(18)30256-X
DOI: <https://doi.org/10.1016/j.jcis.2018.03.014>
Reference: YJCIS 23364

To appear in: *Journal of Colloid and Interface Science*

Received Date: 18 December 2017
Revised Date: 4 March 2018
Accepted Date: 6 March 2018

Please cite this article as: M.E. Alea-Reyes, O. Penon, P. García Calavia, M.J. Marín, D.A. Russell, L. Pérez-García, Synthesis and *in vitro* phototoxicity of multifunctional Zn(II)meso-tetrakis(4-carboxyphenyl)porphyrin-coated gold nanoparticles assembled *via* axial coordination with imidazole ligands, *Journal of Colloid and Interface Science* (2018), doi: <https://doi.org/10.1016/j.jcis.2018.03.014>

This is a PDF file of an unedited manuscript that has been accepted for publication. As a service to our customers we are providing this early version of the manuscript. The manuscript will undergo copyediting, typesetting, and review of the resulting proof before it is published in its final form. Please note that during the production process errors may be discovered which could affect the content, and all legal disclaimers that apply to the journal pertain.



Synthesis and *in vitro* phototoxicity of multifunctional Zn(II)meso-tetrakis(4-carboxyphenyl)porphyrin-coated gold nanoparticles assembled *via* axial coordination with imidazole ligands

María E. Alea-Reyes,^{a,b} Oriol Penon,^{a,b} Paula García Calavia,^c María J. Marín,^c David A. Russell,^{c*} and Lluïsa Pérez-García^{a,b,1*}

^aDepartament de Farmacologia, Toxicologia i Química Terapèutica, Universitat de Barcelona, Avda. Joan XXIII 27-31, 08028 Barcelona, Spain. E-mail: mlperez@ub.edu; malearey7@alumnes.ub.edu; oriolpenon@gmail.com

^bInstitut de Nanociència i Nanotecnologia UB (IN2UB), Universitat de Barcelona, Avda. Joan XXIII 27-31, 08028 Barcelona, Spain.

^cSchool of Chemistry, University of East Anglia, Norwich Research Park, Norwich, Norfolk, NR4 7TJ, UK. E-mail: p.garcia-calavia@icenidiagnostics.com; m.marin-altaba@uea.ac.uk; D.Russell@uea.ac.uk

ABSTRACT

*Corresponding author at: Departament de Farmacologia, Toxicologia i Química Terapèutica, Universitat de Barcelona, 08028 Barcelona, Spain, Telephone: (+34) 934035849. Fax (+34) 934024539
E-mail address: mlperez@ub.edu

¹ Present address: School of Pharmacy, The University of Nottingham, University Park, Nottingham, NG7 2RD, United Kingdom

²Abbreviations: Reactive Oxygen Species (ROS). Photodynamic Therapy (PDT). Gold Nanoparticles (GNP). Singlet Oxygen (¹O₂). Photosensitisers (PS). Dynamic Light Scattering (DLS). High-Resolution Transmission Electron Microscopy (HRTEM). Dimethyl sulfoxide (DMSO). Methanol (MeOH). Dimethylformamide (DMF). Gold (III) chloride trihydrate (HAuCl₄·3H₂O). Methyl imidazole (Im-C₁). Octadecylimidazole (Im-C₁₈). Sodium borohydride (NaBH₄). 1-(11-Mercaptoundecyl)imidazole (Im-C₁₁-SH). (11-Mercaptoundecyl)hexa(ethylene glycol) (HS-C₁₁-(EG)₆-OH). Sodium chloride (NaCl). Sodium phosphate monobasic (NaH₂PO₄). Fetal Bovine Serum (FBS). 9,10-Anthracenediyl-bis(methylene)dimalonic acid (ABMA). Potassium chloride (KCl). Calcium chloride dihydrate (CaCl₂·2H₂O). Magnesium chloride hexahydrate (MgCl₂·6H₂O). 4-(2-Hydroxyethyl)piperazine-4-ethanesulfonic acid (HEPES). Bovine Serum Albumin (BSA), Sodium phosphate dibasic (Na₂HPO₄), Potassium phosphate monobasic (KH₂PO₄). Ethylenediaminetetraacetic acid (EDTA). L-glutamine (L-Gln). Human breast adenocarcinoma cells (SK-BR-3). Hank's Balanced Salt Solution (HBSS). Phosphate buffered saline (PBS). Zn(II)-meso-tetraphenylporphyrin (ZnTPP). Zn(II)meso-tetrakis(4-carboxyphenyl)porphyrin, sodium salt (Na-ZnTCPP). Tetrakis(4-carboxyphenyl)porphyrin, sodium salt (Na-H₂TCPP).

Hypothesis

Metalloporphyrins are extensively investigated for their ability to form reactive oxygen species and as potent photosensitisers for use in photodynamic therapy. However, their hydrophobicity generally causes solubility issues concerning *in vivo* delivery due to lack of distribution and low clearance from the body. Immobilising porphyrins on carriers, such as gold nanoparticles (GNP), can overcome some of these drawbacks. The mode of assembling the porphyrins to the carrier influences the properties of the resulting drug delivery systems.

Experiments

We describe the synthesis and characterisation of new porphyrin decorated water soluble GNP and we explore Zn-imidazole axial coordination as the mode of linking the porphyrin to the metallic core of the nanoparticles. Quantification of singlet oxygen production, toxicity in dark, cellular uptake by SK-BR-3 cells and phototoxicity have been assessed.

Findings

Axial coordination limits the number of porphyrins on the gold surface, reduces the formation of aggregates, and diminishes metal exchange in the porphyrin, all of which contribute to enhance the efficiency of singlet oxygen generation from the immobilised porphyrin. *In vitro* experiments on SK-BR-3 cells reveal a fast uptake followed by more than 80% cell death after irradiation with low doses of light.

Keywords: Zn(II)meso-tetrakis(4-carboxyphenyl)porphyrin; gold nanoparticles; imidazole ligands; Zn(II)-imidazole axial coordination; singlet oxygen production; SK-BR-3 cells; cellular uptake; dark cytotoxicity; phototoxicity; photodynamic therapy.

ACCEPTED MANUSCRIPT

1. Introduction

Porphyrins have been increasingly studied due to their numerous applications in different areas such as photochemistry, molecular recognition, sensors, molecular machines or in photodynamic therapy (PDT).¹⁻³ The presence and the nature of a central metal ion influences the photophysical properties of metalloporphyrins and can lead, as is the case for PDT, to an increased production of reactive oxygen species (ROS) and singlet oxygen ($^1\text{O}_2$) due to the heavy-metal effect.⁴ However, the majority of photosensitisers (PS) used in PDT are hydrophobic, which generally raises solubility concerns when applied in the clinical setting, causing poor biodistribution and low clearance from the body.⁵ Therefore, the use of nanostructured vehicles to transport and deliver such PS can help to overcome this limitation. Nanoparticles are envisaged as powerful platforms for molecular recognition⁶ and they have been used for cancer theranostics following porphyrin coating.⁷ Amongst others, gold nanoparticles (GNP) have been explored as drug delivery carriers for PDT,⁸⁻¹⁰ and they offer an added value since porphyrins are more effective when immobilised on GNP rather than free in solution, showing enhanced $^1\text{O}_2$ production.¹⁰⁻¹² Different parameters influence the $^1\text{O}_2$ generation efficacy of immobilised porphyrins, such as the particle size, the length of the linker, their surface density and their orientation with respect to the gold core.¹³⁻¹⁶ For instance, the fluorescence quantum yield decreases when the average number of coating porphyrins increases.^{13,14} The majority of the examples reported in the literature^{7,13} and by us^{9,11,17,18} describe the self-assembly of thiolated porphyrins onto GNP through synthetic approaches that do not enable a complete control of the surface density and localisation of the coating agents, especially when mixed monolayers are used.

Immobilisation of metalloporphyrins in a well-defined orientation on the GNP surface could bring control to the assembly and improve PDT properties of the nanomaterial. Axial base coordination to metalloporphyrins has been extensively used for the design of self-assembled materials,¹⁹ an interaction exploited at the base of some sensors.²⁰ Here, we explore axial base coordination as the mode of linkage between metalloporphyrins and GNP surfaces. Thus, we designed a multicomponent self-assembled material, the components of which offer different functions and advantages, contributing to improved PDT properties. This multifunctional new water-soluble nanomaterial (**Na-ZnTCPPImGNP**) is formed by a) GNP as the carrier core and as a singlet oxygen generation enhancer, b) a water-soluble Zn-porphyrin as an efficient photosensitiser, capable of axial coordination, c) a thiolated imidazole derivative as the stabiliser agent of gold and the linker to the Zn-porphyrin, of sufficient length (11 carbon atoms spacer) to avoid gold-porphyrin direct interaction, and d) a thiolated polyethyleneglycol co-coating agent, to increase the water solubility of the whole system. We expected that this specific spatial disposition would limit the number of porphyrins on the gold surface,¹³ reduce the formation of aggregates^{21,22} and reduce the possibility of metal exchange of the porphyrin,²² contributing to an enhancement in the efficiency of $^1\text{O}_2$ generation beneficial for PDT.

Different techniques were used to characterise the novel **Na-ZnTCPPImGNP** including UV-visible absorption spectroscopy, dynamic light scattering (DLS), high-resolution transmission electron microscopy (HRTEM) and fluorescence spectroscopy. Several parameters regarding the GNP were investigated, such as the amount of the incorporated photosensitiser, the production of $^1\text{O}_2$ and the PDT activity of the nanosystems. The PDT activity was investigated *in vitro* using SK-BR-3 human breast adenocarcinoma cells by studying cytotoxicity, phototoxicity and intracellular uptake, to provide a water-soluble nanosystem suitable for PDT.

2. Experimental Section

2.1. Materials

Solvents

Dimethyl sulfoxide (DMSO), methanol (MeOH), dimethylformamide (DMF) and toluene were purchased from Sigma Aldrich.

Reagents

Gold (III) chloride trihydrate ($\text{HAuCl}_4 \cdot 3\text{H}_2\text{O}$), methyl imidazole (Im-C₁), octadecylimidazole (Im-C₁₈) and sodium borohydride (NaBH_4) were obtained from Sigma-Aldrich (Germany). 1-(11-Mercaptoundecyl)imidazole (Im-C₁₁-SH) and (11-mercaptoundecyl)hexa(ethylene glycol) (HS-C₁₁-(EG)₆-OH) were purchased from Prochimia (France). Sodium chloride (NaCl), sodium phosphate monobasic (NaH_2PO_4) and fetal bovine serum (FBS) were purchased from Thermo Fisher Scientific (UK). 9,10-Anthracenediyl-bis(methylene)dimalonic acid (ABMA), potassium chloride (KCl), calcium chloride dihydrate ($\text{CaCl}_2 \cdot 2\text{H}_2\text{O}$), magnesium chloride hexahydrate ($\text{MgCl}_2 \cdot 6\text{H}_2\text{O}$), 4-(2-hydroxyethyl)piperazine-4-ethanesulfonic acid (HEPES), bovine serum albumin (BSA), sodium phosphate dibasic (Na_2HPO_4), potassium phosphate monobasic (KH_2PO_4) and propidium iodide were purchased from Sigma-Aldrich (UK). Trypsin 0.25% with ethylenediaminetetraacetic acid (EDTA) and McCoy's 5A phenol red-free medium containing L-glutamine (L-Gln) were purchased from Invitrogen (UK). CellTiter-Blue® cell viability assay was purchased from Promega (UK). 75 cm² Nunc Easy tissue culture flasks with porous caps, Nunc Nunclon™ Surface 6-well multidishes, Nunc Nunclon™ Surface 96-well white-bottom microplates and 18 mm diameter glass coverslips were purchased from Thermo Fisher (UK).

SK-BR-3 human breast adenocarcinoma cells were purchased from LGC Standards and kindly provided by Prof Dylan R. Edwards (Norwich Medical School, University of East Anglia, UK).

2.2. Characterisation methods

UV-visible absorption spectra were obtained using a UV-1800 Shimadzu UV spectrophotometer. The samples were placed in quartz cuvettes with a 1 cm path length. Absorption spectra were determined in toluene or water. Fluorescence excitation and emission spectra were recorded using a Hitachi F-4500 fluorescence spectrometer. The spectra were recorded using quartz cuvettes with a 1 cm path length. High-Resolution Transmission Electron Microscopy (HRTEM) images were obtained using a JEOL JEM 2100 transmission electron microscope at 200 kV from *Centres Científics i Tecnològics Universitat de Barcelona* (CCiT-UB). The images were captured by a Megaview III Soft Imaging System camera and the size of the gold nanoparticles was measured with ImageJ. The size of the nanoparticles was also determined by Dynamic Light Scattering (DLS) using a Zetasizer Nano ZS series (Malvern Instruments). Thermogravimetric analysis (TGA) was performed on Mettler Toledo TGA/SDTA 851e, from 30 °C to 700 °C with a heating rate of 5 °C min⁻¹, from CCiT-UB. Capsules: crucible of aluminium (100 µL) with perforated cap. Nitrogen was used as purgative gas in all of the measurements. SK-BR-3 cells were imaged using a Zeiss Axiovert 200M microscope. Fluorescence images were captured using a 63x PlanApochromat (1.4 NA) oil-immersion objective lens, a Zeiss AxioCamMRm CCD camera and AxioVision software. Images were collected and processed using the AxioVision SE64 Rel. 4.8 software.

2.3. Synthesis and characterisation of Na-ZnTCPPImGNP

A solution of H₂AuCl₄·3H₂O (3.6 mg, 0.009 mmol) in water (1.0 mL) was added to a stirred solution of 11-mercaptoundecyl hexa(ethylene glycol) (HS-C₁₁-(EG)₆-OH) (4.2 mg,

0.008 mmol) and thiol-imidazole Im-C₁₁-SH (6.9 mg, 0.027 mmol) in MeOH (2.0 mL). Then, an excess of NaBH₄ (5.3 mg, 0.14 mmol) in water (1.0 mL) was added dropwise to the mixture, while the solution changed to a dark red colour. The reaction was allowed to occur under stirring at room temperature overnight. After this time, the residue containing the **ImGNP** was washed with water (3x5mL) by centrifugation (14,500 rpm, 15 min at 15 °C, LabnetPrismR centrifuge). A brown solution was obtained as **ImGNP**, which was characterised by UV-visible absorption spectroscopy and HRTEM. Then, a solution of **ImGNP** (1 mL, 7.1×10⁻³ μM) in water was added to an aqueous solution of **Na-ZnTCPP** (1.6 ×10³ μM) and the mixture was stirred at room temperature overnight. The residue, containing the **Na-ZnTCPPImGNP**, was washed with water (3x5mL) by centrifugation (14,500 rpm, 15 min at 15 °C, LabnetPrismR centrifuge). The purified nanoparticles **Na-ZnTCPPImGNP** were characterised by UV-visible absorption and fluorescence spectroscopies, and HRTEM.

2.4. Singlet oxygen production of the Na-ZnTCPP and Na-ZnTCPPImGNP

Singlet oxygen production was measured using the singlet oxygen probe 9,10-anthracenediyl-bis(methylene)dimalonic acid (ABMA). ABMA is photobleached in the presence of ¹O₂ to give a non-fluorescent 9,10-endoperoxide product. The photobleaching can be monitored by fluorescence spectroscopy. A solution of ABMA (0.2 mg, 0.51 mM) in MeOH (1 mL) was prepared. Then 3 μL of this solution was added to a quartz cuvette containing either **Na-ZnTCPP** (4.34 μL, 3 μM) or **Na-ZnTCPPImGNP** (484 μL, 3 μM of incorporated porphyrin) in water. The final volume (1.5 mL) in the cuvettes was completed with water and the solutions were thoroughly stirred. A light source in the range 400-500 nm was used to irradiate the mixtures during 4 h, using a power of 0.16 mW/cm². The light source was located 3 cm away from the cuvette. Fluorescence emission spectra were recorded every hour between 390-600 nm,

following excitation at 380 nm. Singlet oxygen production was determined by the decrease of the fluorescence emission intensity of ABMA at 431 nm.

2.5. Biological experiments

Imaging medium

The imaging medium based on Hank's balanced salt solution (HBSS) used for the biological experiments was prepared in water containing NaCl (120 mM), KCl (5 mM), CaCl₂·2H₂O (2 mM), MgCl₂·6H₂O (1 mM), NaH₂PO₄ (1 mM), NaHCO₃ (1 mM), HEPES (25 mM), D-glucose (11 mM) and BSA (1 mg/mL). The pH of the imaging medium was adjusted to 7.4 using an aqueous solution of NaOH (1 M). The imaging medium was sterilised-filtered through a Millex GP syringe driven filter unit (0.22 µm) prior to use.

Phosphate buffered saline (PBS)

The PBS solution used for the biological experiments was prepared by dissolving 10 PBS tablets in water (1 L). The solution was sterilised by autoclaving at 110 °C for 10 min. The newly prepared PBS solution contained Na₂HPO₄ (8 mM), KH₂PO₄ (1 mM), NaCl (160 mM) and KCl (3 mM) with a pH value of 7.3.

Propidium iodide solution in PBS

A solution of propidium iodide (1 mg/mL) was prepared in PBS. The PBS buffer (10 mM) used was prepared using NaH₂PO₄·2H₂O and Na₂HPO₄ stock solutions (200 mM). The PBS solution contained NaCl (150 mM) and CaCl₂·2H₂O (100 µM). The pH of the PBS was adjusted to 7.4 using aqueous solutions of NaOH (1 M) and HCl (0.6 M). Prior to use, the propidium iodide solution was sterilised by filtration through a 0.22 µm filter unit.

Culture of SK-BR-3 cells

SK-BR-3 cells were routinely cultured in phenol red-free McCoy's 5A medium containing L-Gln and supplemented with FBS (10%). The cells were grown in 75 cm² Nunc Easy tissue culture flasks at 37 °C under a 5% CO₂ atmosphere. SK-BR-3 cells were subcultured (1:4) every 5 days, when they reached near confluence. The culture medium was discarded and the cells were washed with PBS (5 mL). The cells were dislodged from the flasks by addition of trypsin 0.25% (1x) EDTA (5 mL) and incubation for 5 min at 37 °C under a 5% CO₂ atmosphere. Trypsin was deactivated by addition of McCoy's 5A medium (5 mL) and removed by centrifugation at 800 rcf for 5 min at 21 °C using an Eppendorf 5810R Centrifuge. The supernatant was removed and the pellet containing the cells was resuspended in McCoy's 5A medium (8 mL) and transferred to two 75 cm² culture flasks.

CelTiter-Blue® cell viability assay

The SK-BR-3 cells were seeded on a white-bottom Nunc Nunclon™ Δ Surface 96 well multidish at a density of 8×10⁴ cells per well in phenol red-free McCoy's 5A medium containing FBS (10%) and L-Gln. The cells were incubated for 48 h at 37 °C under a 5% CO₂ atmosphere. The medium was then removed and the cells were washed once with PBS (100 μL). The cells were incubated with **Na-ZnTCPPImGNP** at either 1.5 μM or 1.75 μM of incorporated porphyrin in FBS-free, phenol red-free McCoy's 5A medium (50 μL) containing L-Gln for 3 h at 37 °C under a 5% CO₂ atmosphere. Additionally, a solution of Staurosporine (1 mM in DMSO) dispersed in FBS-free, phenol red-free McCoy's 5A medium containing L-Gln (50 μL; 20 μM) was used as a positive control for cytotoxicity. Following incubation, the medium was removed and the cells were washed three times with PBS (100 μL) to remove all non-internalised GNP. The cells were kept in phenol red-free McCoy's 5A medium (100 μL) containing FBS (10%) and L-Gln. At this point, some of the cells were irradiated using a light

source with a power of 2.54 mW/cm^2 and an excitation wavelength between 400 and 500 nm. The cells were irradiated for 10, 20 or 30 min per well. The light source was located 1 cm above the 96 well plates. The wells not being irradiated were left covered with aluminum foil so that the light would not affect them. Once all the wells were irradiated, the cells were further incubated for 48 h at 37°C under a 5% CO_2 atmosphere. CellTiter-Blue® reagent (20 μL) was added to each well and incubated for 4 h at 37°C under a 5% CO_2 atmosphere. Fluorescence emission intensity in the wells was then measured at 590 nm following excitation at 560 nm using a CLARIOstar® (BMG Labtech) microplate reader. Background fluorescence was corrected by subtracting the fluorescence emission of phenol red-free McCoy's 5A medium incubated with CellTiter-Blue®. Cell viability was calculated as a percentage of non-treated, non-irradiated cells. The samples were analysed in triplicate. Control cells without **Na-ZnTCPPImGNP** loaded were treated with FBS-free, phenol red-free McCoy's 5A medium during the 3 h incubation period. Furthermore, control cells were only irradiated for 30 min to assess the direct effect of the blue light source on the cells.

Treatment of SK-BR-3 cells to study internalisation and PDT effect of Na-ZnTCPPImGNP

For imaging, SK-BR-3 cells were cultured on sterile 18 mm diameter glass coverslips inside Nunc 6-well multidishes at a density of 2×10^4 cells/mL (3 mL/well) at 37°C under a 5% CO_2 atmosphere 48 h prior to performing imaging experiments.

The growth medium of the SK-BR-3 cells on the coverslip was removed. The cells were then washed with PBS (1 mL) once. For samples treated with the **Na-ZnTCPPImGNP**, a solution of the **Na-ZnTCPPImGNP** (1 mL) in FBS-free, phenol red-free McCoy's 5A medium containing L-Gln at either 1.5 μM or 1.75 μM was added to the coverslip. For control cells, FBS-free, phenol red-free McCoy's 5A medium containing L-Gln (1 mL) was added to the coverslip. The

cells were then incubated for 3 h at 37 °C under a 5% CO₂ atmosphere. Following incubation, the cells were washed three times with PBS (1 mL) and kept in phenol red-free McCoy's 5A medium containing FBS (10%) and L-Gln (2 mL).

At this point, some of the cells were irradiated using the light source (400 – 500 nm) with a power of 2.54 mW/cm² for 30 min per well. The light source was located 1 cm above the plates. The wells not being irradiated were left covered with aluminum foil so the light would not affect them. All the cells the cells were further incubated for *ca.* 72 h at 37 °C in a 5% CO₂ atmosphere.

Imaging of SK-BR-3 cells using a fluorescence microscope

For imaging, the 18 mm coverslip containing the SK-BR-3 cells was placed in a Ludin chamber (Life Imaging Service, Olten, Switzerland), which was securely tightened. Each coverslip was washed three times with imaging medium (*ca.* 1 mL) and finally resuspended in imaging medium (*ca.* 1 mL). The Ludin chamber was fitted on a heating stage at 37 °C in a Zeiss Axiovert 200M fluorescence microscope. The images were acquired with a 63x Plan Aplanachromat (1.4 NA) oil-immersion objective. **Na-ZnTCPPImGNP** internalised by the cells were excited at 530-585 nm and the fluorescence emission was collected in the red channel through a 600 nm long-pass filter. To evaluate the PDT effect, propidium iodide (5 µL, 1 mg/mL in PBS) was mixed with imaging medium (1 mL). The solution was directly added to the coverslip already placed in the Ludin chamber and incubated at 37 °C in the dark on the heating stage of the fluorescence microscope for *ca.* 5 min. The propidium iodide was excited at 530-585 nm and the fluorescence emission was collected in the red channel through a 600 nm long-pass filter.

3. Results and Discussion

The structures of the porphyrins used in this work are shown in Fig. 1a, and they were synthesised following protocols previously reported.²³⁻²⁷ An imidazole based ligand for axial coordination was selected, because imidazole derivatives bind more strongly than pyridine derivatives to Zn-porphyrins.²⁸⁻³⁰ In order to select the optimum components to be used in the subsequent preparation of **Na-ZnTCPPImGNP** exploiting axial coordination, the complexation in solution was evaluated between the model porphyrin **ZnTPP** (in toluene) or **Na-ZnTCPP** (in water) and different alkylimidazoles: methyl imidazole (Im-C₁), 1-(11-mercaptopundecyl)imidazole (Im-C₁₁-SH) and octadecylimidazole (Im-C₁₈) (Fig. 1b). The complexation study was analysed using UV-visible absorption spectroscopy and the results (as seen in ESI Fig. S1-S3) were in agreement with previously reported data^{19,28-30} and confirmed the coordinationability between the central Zn atom in both porphyrins and the different imidazole derivatives. Also, the titration experiments in aqueous solution revealed that there is no significant influence of the chain length of the imidazole connector upon coordination to **Na-ZnTCPP**. Subsequently, the sodium salts of porphyrins tetrakis(4-carboxyphenyl)porphyrin (**Na-H₂TCPP**) and Zn(II)meso-tetrakis(4-carboxyphenyl)porphyrin (**Na-ZnTCPP**) were used as photosensitisers and were immobilised on water-soluble nanoparticles.

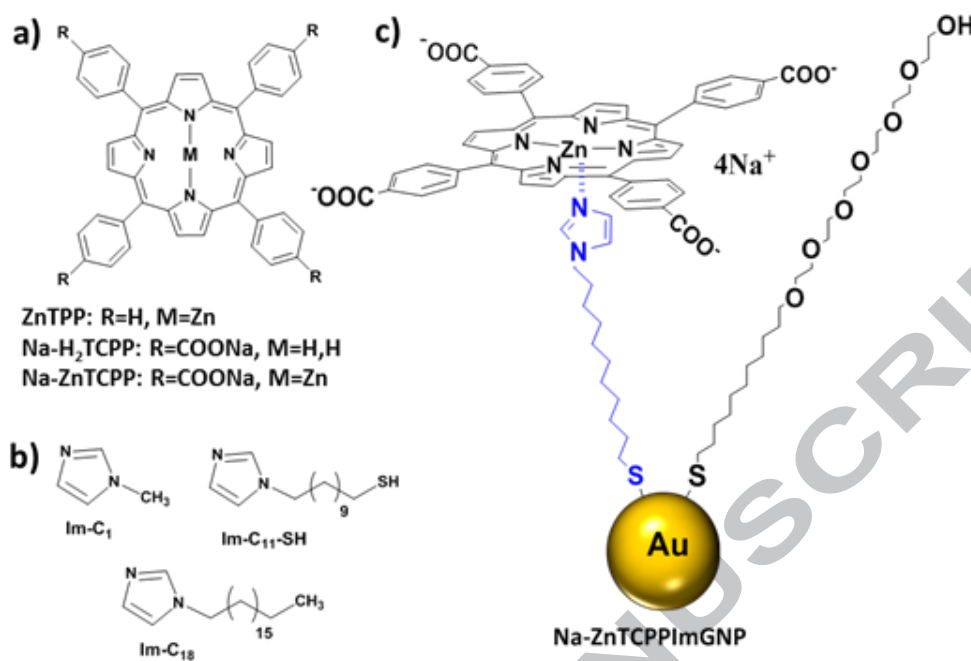


Fig. 1. Structures of: a) Porphyrins ZnTPP , $\text{Na-H}_2\text{TCPP}$ and Na-ZnTCPP , b) imidazole derivatives (Im-C_1 , $\text{Im-C}_{11}\text{-SH}$ and Im-C_{18}) and c) schematic representation of Na-ZnTCPPImGNP .

3.1. Synthesis and characterisation of Na-ZnTCPPImGNP

Taking into account the coordination results, where the ability of the $\text{Im-C}_{11}\text{-SH}$ to coordinate with Na-ZnTCPP was proven, the possibility to incorporate Na-ZnTCPP into imidazole modified ImGNP was tested.

$\text{Im-C}_{11}\text{-SH}$ was chosen to be integrated in the Na-ZnTCPPImGNP (Fig. 1c) due to its high affinity for the metalloporphyrin of interest.^{19,31,32} The thiol group present in the $\text{Im-C}_{11}\text{-SH}$ allows assembly to the gold surface of the GNP, facilitating their synthesis, stabilisation and subsequent incorporation of the photosensitiser Na-ZnTCPP upon axial coordination. Imidazole functionalised gold nanoparticles ImGNP were synthesised using a mixture of thiols $\text{HS-C}_{11}\text{-(EG)}_6\text{-OH}$ and $\text{Im-C}_{11}\text{-SH}$ as the stabilising agents; the thiol $\text{HS-C}_{11}\text{-(EG)}_6\text{-OH}$ provides water solubility and $\text{Im-C}_{11}\text{-SH}$ acts as the connector for the subsequent coordination of Zn-porphyrins.

The UV-visible absorption spectra of the **ImGNP** showed a strong absorption band at approximately 526 nm, originated from the surface plasmon absorption of nanosized GNP (Fig. 2a red line). These **ImGNP** were characterised by high-resolution transmission electron microscopy (HRTEM) to study their morphology and size distribution as seen in ESI Fig. S4a; **ImGNP** displayed a cubeoctahedron shape and a low polydispersity with an average size of 8 nm (ESI Fig. S4a and c). Then, the synthesis of **Na-ZnTCPPImGNP** was carried out by mixing **ImGNP** and **Na-ZnTCPP** in water. **Na-ZnTCPPImGNP** were characterised by UV-visible absorption spectroscopy (Fig. 2a blue line). The absorption spectrum of **Na-ZnTCPPImGNP** exhibited the surface plasmon band of GNP at *ca.* 520 nm and the porphyrin Soret band at *ca.* 430 nm. The Soret band of the **Na-ZnTCPP** coordinated to the gold nanoparticles is red-shifted compared to that of the free **Na-ZnTCPP** ($\lambda = 420$ nm; Fig. 2a black line) due to the coordination between the Zn-porphyrin and the imidazole moieties on the GNP. In addition, the UV-visible absorption spectrum of the **Na-ZnTCPPImGNP** shows an indication of the presence of the two typical zinc porphyrin Q bands at 564 and 608 nm. Furthermore, **Na-ZnTCPPImGNP** display a cubeoctahedron shape and a low polydispersity with an average size of 8 nm as shown in Fig. 2b and in ESI Fig. S4b and d.

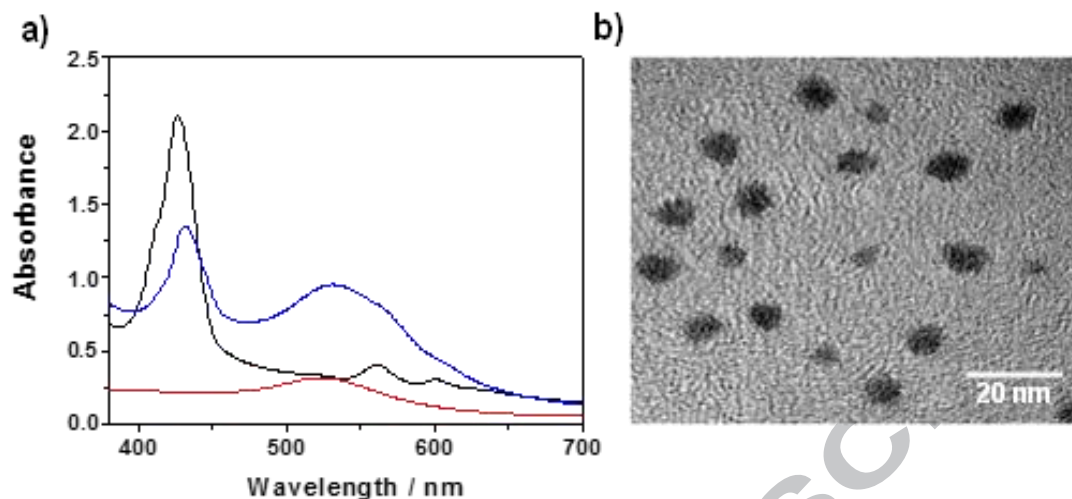


Fig. 2. a) UV-visible absorption spectra of the free porphyrin **Na-ZnTCPP** (black line), **ImGNP** (red line) and **Na-ZnTCPPImGNP** (blue line) recorded in water and b) HRTEM image of **Na-ZnTCPPImGNP**.

The size of **ImGNP** and **Na-ZnTCPPImGNP** was also measured using dynamic light scattering (DLS). Both types of nanoparticles proved stable in solution and have low polydispersity with an average hydrodynamic size between 13.5-15.4 nm. The nanoparticle diameter obtained by DLS is larger than that obtained by HRTEM. In HRTEM, only the size of the gold core was measured since no contrast agent was used and the surrounding ligands are transparent to the electron beam. On the contrary, DLS measures the hydrodynamic size of the nanoparticles. Therefore, the size measured by DLS gives the diameter that includes not only the core but also the alkyl chains of the ligands. **Na-ZnTCPPImGNP** showed the largest size (15.4 nm), this result is likely due to the porphyrin coordinated with the imidazole Im-C₁₁-SH on the surface of **Na-ZnTCPPImGNP**, which leads to an increase in the hydrodynamic diameter of the nanoparticles.

The fluorescence emission spectra of both **Na-ZnTCPP** and **Na-ZnTCPPImGNP** were recorded in water (see ESI Fig. S5), and both exhibited two emission bands at $\lambda = 604$ and $\lambda = 655$ nm following excitation at 421 nm, as expected for Zn-porphyrin derivatives.³³ In the case of the coated gold nanoparticles **Na-ZnTCPPImGNP** a decrease in the emission intensity with respect to the spectrum of the free porphyrin was observed, indicating the successful immobilisation of the porphyrin **Na-ZnTCPP** through axial coordination with the imidazole derivative on the GNP.³⁴

To differentiate axial coordination from unspecific immobilisation, we also synthesised nanoparticles using the porphyrin that did not contain zinc, **Na-H₂TCPP**, yielding **Na-H₂TCPPImGNP** (see Section 2 in ESI). As shown in ESI Fig. S6a, the UV-visible extinction spectrum of the **Na-H₂TCPPImGNP** shows a small band at 420 nm, corresponding to the incorporated **Na-H₂TCPP** porphyrin, and showing no shift compared to the free **Na-H₂TCPP** in solution. The incorporation of **Na-H₂TCPP** onto **ImGNP** could be attributed to non-specific interactions such as those between the alkylimidazole coating and the porphyrin. Instead, the absorption spectrum of **Na-ZnTCPPImGNP** reveals an intense band at 430 nm due to the corresponding porphyrin **Na-ZnTCPP** axially incorporated (see ESI Fig. S6b), showing a red shift compared to the free **Na-ZnTCPP** in solution (λ *ca.* 423 nm), which indicates that the porphyrin is located in a more hydrophobic environment as a consequence of a strong imidazole-zinc coordination.³⁴ This experiment demonstrates that the presence of the metal within the core of the porphyrin is essential for the axial coordination to the imidazole moiety linked to the GNP,^{19,31,35,36} thus facilitating the incorporation of the porphyrin on the GNP on a spatially controlled manner.

The amount of porphyrin, **Na-H₂TCPP** or **Na-ZnTCPP**, per nanoparticle was estimated using UV-visible absorption spectroscopy (see ESI Fig. S6) and the calculations reported by Haiss *et al.*³⁷ Using the extinction coefficient calculated for **Na-H₂TCPP** (see ESI Fig. S7), the reported for **Na-ZnTCPP**³⁸ and the concentration of GNP in the sample, a ratio of the porphyrin per nanoparticle can be estimated as shown in ESI Fig. S8 and Table S1, which shows all the data obtained from the UV-visible absorption spectra shown in ESI Fig. S6 that was used to estimate the ratio between the porphyrins and GNP. First, the absorbance at 420 nm (**Na-H₂TCPP**) or 430 nm (**Na-ZnTCPP**) corresponding to the porphyrins' Soret band needs to be normalised to remove the influence from the GNP absorption spectrum. To calculate the contribution of the porphyrin ligands to the absorbance at 420 nm, the intensity corresponding to the GNP at 460 nm (**Na-H₂TCPPImGNP**) or 480 nm (**Na-ZnTCPPImGNP**) should be subtracted from the total intensity at 420 nm or 430 nm, respectively. Secondly, Avogadro's number, the volume per cuvette (3 mL) and the GNP diameter, which was previously obtained by HRTEM, can be used to calculate the number of porphyrin molecules per GNP (see ESI Fig. S8 and Table S1).

The values shown in ESI Table S1 prompted us to calculate the number of porphyrin molecules immobilised on the **Na-H₂TCPPImGNP** and **Na-ZnTCPPImGNP**, corresponding to 186 **Na-H₂TCPP** molecules/ GNP and 106 **Na-ZnTCPP** molecules/ GNP, respectively. A difference of the ratio of both immobilised porphyrins was obtained, indicating that the presence of the zinc on the porphyrin decreases the porphyrin incorporation due to its well-defined orientation associated to spatial constraints, including the contribution of the pegylated coating agent to steric hindrance, being its coordination with the imidazole moieties in the GNP what directs its ordered assembly around the gold core.

Additionally, thermogravimetric analysis (TGA) of **Na-ZnTCPPImGNP** was performed (see ESI Fig. S9) in an attempt to determine the presence of porphyrin into gold nanoparticles in more than one binding mode, due to the excess of porphyrin used in the synthesis of the gold nanoparticle, but the results are not conclusive, since the porphyrin used (**Na-ZnTCPP**) is a salt and a clear loss of mass is not expected to be seen clearly. The thermogram included in Fig. S9 SI shows two main intervals of mass loss, probably corresponding to the loss of the two different thiolated species anchored on the gold surface. The second interval is quite wide because at this temperature range probably the porphyrin starts decomposing, so its mass loss is concomitant to the thiolated linker loss.

3.2. Singlet oxygen production by **Na-ZnTCPP** and **Na-ZnTCPPImGNP**

The singlet oxygen production of **Na-ZnTCPP** and **Na-ZnTCPPImGNP** was examined using anthracenediyl-bis(methylene)dimalonic acid (ABMA), a water-soluble anthracene derivative that reacts selectively with $^1\text{O}_2$. Upon reaction with $^1\text{O}_2$, ABMA is photobleached leading to the formation of a non-fluorescent 9,10-endoperoxide product.^{17,38} The reaction between ABMA and $^1\text{O}_2$ can thus be monitored using fluorescence spectroscopy. The photosensitiser **Na-ZnTCPP** and the **Na-ZnTCPPImGNP** were irradiated, in the presence of ABMA, with a blue light source (400 – 500 nm), which excites the Soret band of the porphyrin (*ca.* 420 nm), for 4 h with continuous stirring. Fluorescence emission spectra were recorded every hour and the singlet oxygen production was determined by the decrease in the fluorescence intensity of ABMA at 431 nm (see ESI Fig. S10). Fig. 3a shows the percentage of photobleaching decay of ABMA at 431 nm following irradiation of the free **Na-ZnTCPP** (red line) and **Na-ZnTCPPImGNP** (blue line). As controls, the singlet oxygen production of **ImGNP** and ABMA were also monitored under the same conditions (see ESI Fig. S10) The

production of singlet oxygen by the **ImGNP** and by the ABMA probe was much lower than for the porphyrin containing nanoparticles (Fig. 3a, green and black line, respectively). These results confirm that the presence of the porphyrin photosensitiser is required to produce $^1\text{O}_2$ upon irradiation. After a 4 hour irradiation period, the percentage of ABMA decay for **Na-ZnTCPP** was *ca.* 22% (Fig. 3, red line), while for the **Na-ZnTCPPImGNP** was *ca.* 56% (Fig. 3, blue line). The $^1\text{O}_2$ production of the free porphyrin **Na-ZnTCPP** is lower than that of the corresponding functionalised **Na-ZnTCPPImGNP**, a feature observed previously for similar systems^{10–12,17,38} which may be attributed to the high localised plasmonic field generated in the gold surface that enhances ROS production.¹⁰

To further compare the ability of both the free porphyrin **Na-ZnTCPP** and the functionalised **Na-ZnTCPPImGNP** to produce singlet oxygen, the maximum rate of ABMA photobleaching was normalised using Equation 1^{17,38} where the concentration of photosensitiser is 3 μM and IF_{431} is the fluorescence emission intensity at 431 nm.

Maximum rate of ABMA photobleaching

$$= \frac{(\%IF_{431} \text{ at } t = 0 \text{ min}) - (\%IF_{431} \text{ at } t = 60 \text{ min})}{60 \text{ min} \times [\text{porphyrin}](\mu\text{M})} \quad (\text{Eq. 1})$$

The calculated maximum rates of ABMA photobleaching following irradiation are reported in Fig. 3b. The value obtained for the free porphyrin **Na-ZnTCPP** was 0.03% IF/(min· μM), while the **Na-ZnTCPPImGNP** showed a higher value of 0.11% IF/(min· μM) photobleaching. These results further confirm that the porphyrins are more effective for the production of singlet oxygen when coordinated to **ImGNP**. The higher production of singlet oxygen for **Na-ZnTCPPImGNP** than for the free porphyrin is remarkable considering that the photobleaching of the **Na-**

ZnTCPPImGNP has been measured in an aqueous solution, where oxygen is less soluble and thus its lifetime is shorter.³⁹

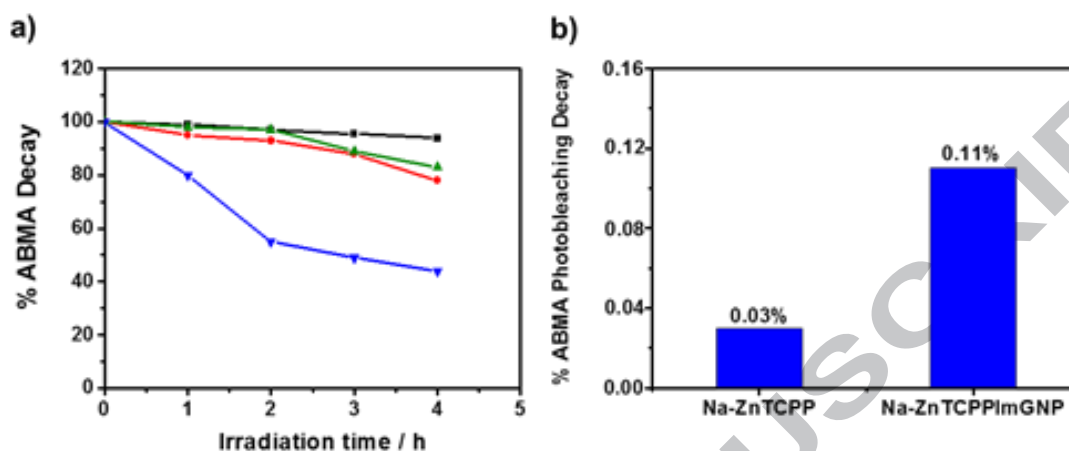


Fig.3. a) Percentage decay of ABMA measured at 431 nm following irradiation (400-500 nm) of: AMBA (■ black line), Na-ZnTCPP (● red line), ImGNP (▲ green line) and Na-ZnTCPPImGNP (◄ blue line). b) Maximum rate of ABMA photobleaching at 431 nm following a 1 h irradiation period, after normalisation of the porphyrin concentration.

3.3. *In vitro* experiments using SK-BR-3 breast cancer cells

The cytotoxic and phototoxic effects of **Na-ZnTCPPImGNP** when the nanoparticles were used to treat SK-BR-3 human breast adenocarcinoma cells were evaluated. The CellTiter-Blue® cell viability assay has been used and recommended to test the cytotoxicity of gold nanoparticles.^{40,41} SK-BR-3 cells were treated with **Na-ZnTCPPImGNP** at two different concentrations of incorporated porphyrin (1.5 μM and 1.75 μM), for 3 h. Following incubation, the cells were washed and irradiated at three different irradiation times *ie.* 10, 20 and 30 min, using a light source of 400 and 500 nm with a power of 2.54 mW/cm^2 .

Cell viability was measured 48 h after PDT treatment, and the results are shown in Fig. 4. When the control cells with no nanoparticles loaded were irradiated during 30 min, the viability

remained high (*ca.* 99%), indicating non-toxicity due to the irradiation with the light source. Following incubation with **Na-ZnTCPPImGNP** at either 1.5 μM (Fig. 4 a) or 1.75 μM (Fig. 4 b) of incorporated photosensitiser, low dark toxicity was observed as the viability of the non-irradiated cells remained at *ca.* 100% and 90%, respectively. Following irradiation, the viability of the SK-BR-3 cells treated with **Na-ZnTCPPImGNP** decreased. This decrease was concomitant with the increase in the concentration of the photosensitiser as well as with the increase in the irradiation time that the cells were subjected to. Cell death was higher (> 60%) at all of the irradiation times used, when the cells were incubated with 1.75 μM **Na-ZnTCPPImGNP**. Superior results were obtained when the cells were incubated with 1.75 μM (incorporated porphyrin) **Na-ZnTCPPImGNP** and subjected to a 30 min irradiation period, reaching cell death values of over 80%. These results confirm that the **Na-ZnTCPPImGNP** synthesised in this study are good candidates for PDT as they induce cell death only following activation with a blue light source.

Reports in the literature present different models of studies of PDT applied with photosensitisers coupled to nanoparticles.^{11,42,43} The main results are studies conducted in different cancer cell-lines, varying irradiation time, doses of light and concentration of the photosensitiser.⁴⁴⁻⁴⁶ Most of these studies suggest that there is a percentage of cell death equal or higher to 90% after having received PDT. Similar results were obtained in this work using SK-BR-3 cells treated with **Na-ZnTCPPImGNP** and using lower doses of light.

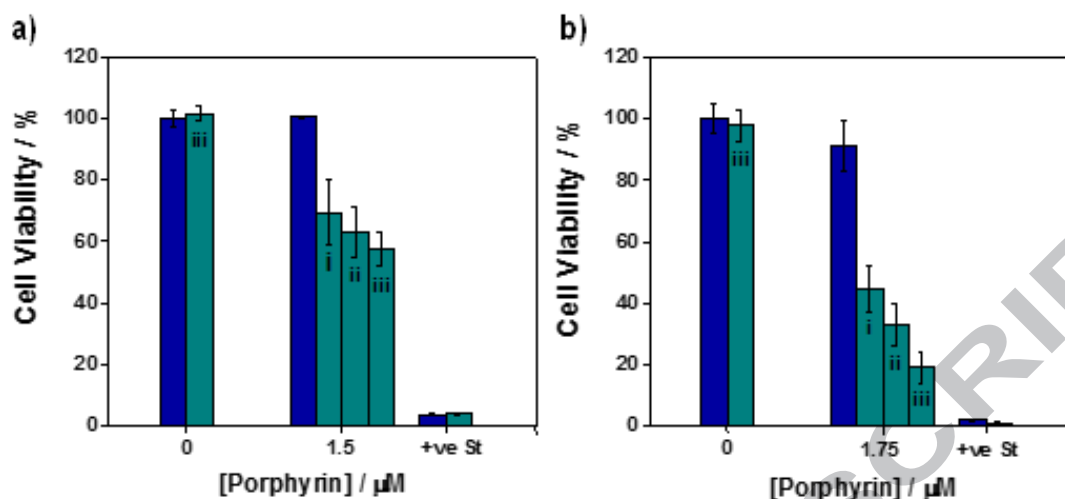


Fig. 4. CellTiter-Blue® cell viability assay results of SK-BR-3 cells incubated with **Na-ZnTCPPImGNP** at either a) 1.5 μM or b) 1.75 μM of incorporated porphyrin **Na-ZnTCPP**. Cells were either irradiated with a blue light source (400-500 nm, dark cyan columns) or non-irradiated (blue columns). The irradiated cells were irradiated for 10 (i), 20 (ii) or 30 (iii) min. Control cells without **Na-ZnTCPPImGNP** loaded were treated with FBS-free, phenol red-free McCoy's 5A medium during the 3 h incubation period and only irradiated for 30 min (iii). The sample +ve St refers to Staurosporine, a positive control for cytotoxicity. Error bars represent the standard deviation with a 95% confidence interval, $n=3$.

3.4. Cellular uptake and phototoxicity of **Na-ZnTCPPImGNP** in SK-BR-3 breast cancer cells using fluorescence microscopy

Internalisation and phototoxicity of **Na-ZnTCPPImGNP** at a concentration of 1.75 μM of incorporated porphyrin were studied in SK-BR-3 breast cancer cells using fluorescence microscopy. The samples were excited at 530-585 nm and the fluorescence emission due to the internalised **Na-ZnTCPPImGNP** was collected in the red channel through a 600 nm long-pass filter. Cells incubated with the **Na-ZnTCPPImGNP** (1.75 μM) for 3 h exhibited a strong intracellular fluorescence due to the **Na-ZnTCPP**, indicating the uptake of the nanoparticles by

the SK-BR-3 cells as shown in Fig. S11a-c. On the other hand, control cells only treated with FBS-free, phenol red-free McCoy's 5A medium showed no fluorescence as shown in Fig. S11d-f. The images in Fig. S11 clearly demonstrate the cellular uptake of the **Na-ZnTCPPImGNP** by the SK-BR-3 breast cancer cell line. Furthermore, cells imaged after being treated with **Na-ZnTCPPImGNP** or corresponding media for 3 h and then incubated for a longer period of time (*ca.* 72 h) also exhibited similar aspect, as seen in Fig. 5, with no apparent morphological changes and therefore, no signs of toxicity in darkness.

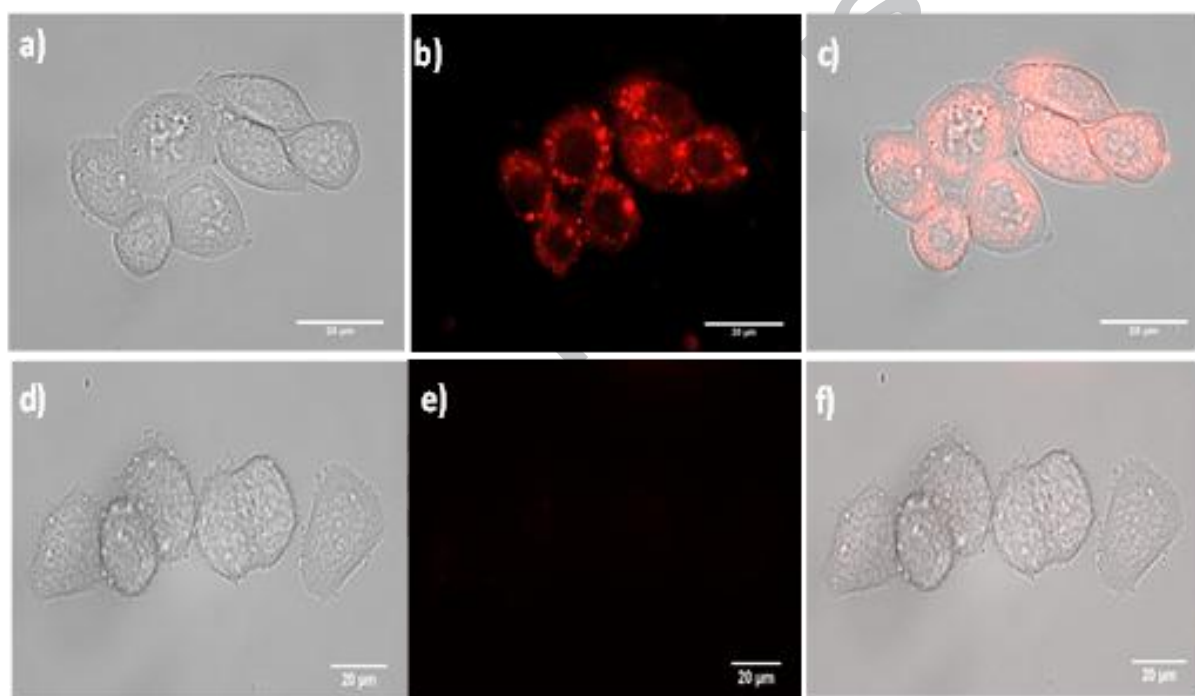


Fig. 5. Brightfield and fluorescence images of non-irradiated SK-BR-3 cells: a)-c) loaded with 1.75 μM **Na-ZnTCPPImGNP** and d)-f) control without nanoparticles loaded. The cells were treated with **Na-ZnTCPPImGNP** or corresponding media for 3 h and then incubated for 72 h prior to imaging. Images correspond to: a) and d) brightfield images; b) and e) fluorescence images due to the fluorescence of the porphyrin on the **Na-ZnTCPPImGNP**; and c) and f) composite images of brightfield and fluorescence. The samples were excited at 530-585 nm and the fluorescence emission was collected in the red channel through a 600 nm long-pass filter. Scale bars = 20 μm .

To study the phototoxicity of the nanoparticles, SK-BR-3 cells were treated with **Na-ZnTCPPIImGNP** (1.75 μM of **Na-ZnTCPP**), irradiated with a blue light source (400-500 nm) for 30 min to induce singlet oxygen production, and incubated for *ca.* 72 h prior to imaging. Changes in the cell morphology of the treated cells were observed (Fig. 6a-c), which were not seen in control cells irradiated for 30 min but not loaded with nanoparticles (Fig. 6d-f). Furthermore, the distribution of the nanoparticles within the cells seems to be different for the irradiated cells (Fig. 6b) as compared to non-irradiated cells that had been treated with **Na-ZnTCPPIImGNP** for 3 h and incubated for 72 h prior to imaging (Fig. 5). The nanoparticles seem to move towards the nucleus of the dead cells following PDT.

To confirm the cell death of those SK-BR-3 cells incubated with **Na-ZnTCPPIImGNP** and irradiated with a 400-500 nm light source for 30 min, the dead cell marker propidium iodide was added to the samples and the cells imaged using the fluorescence microscope. Propidium iodide is cell-impermeable thus it can only intercalate with the DNA in the nucleus of those cells where the membrane has been damaged.⁴⁷ Therefore, propidium iodide can stain dead cells.⁴⁸ As shown in Fig. 6g-i, high fluorescence emission from the nucleus of the cells incubated with the **Na-ZnTCPPIImGNP** and irradiated to induce production of singlet oxygen was observed in the red channel. Control cells, without **Na-ZnTCPPIImGNP** loaded and irradiated with a 400-500 nm light source for 30 min, did not exhibit fluorescence emission in the red channel (Fig. 6j-l) due to the propidium iodide. Furthermore, the intensity of the red fluorescence after addition of propidium iodide (Fig. 6h) is significantly higher than prior to addition (Fig. 6b), indicating positive propidium iodide staining. Additionally, as previously mentioned, changes in the cell morphology suggest that the SK-BR3 cells loaded with **Na-ZnTCPPIImGNP** experienced PDT-induced cell death, a result in agreement with the cell viability assay reported in Fig. 4.

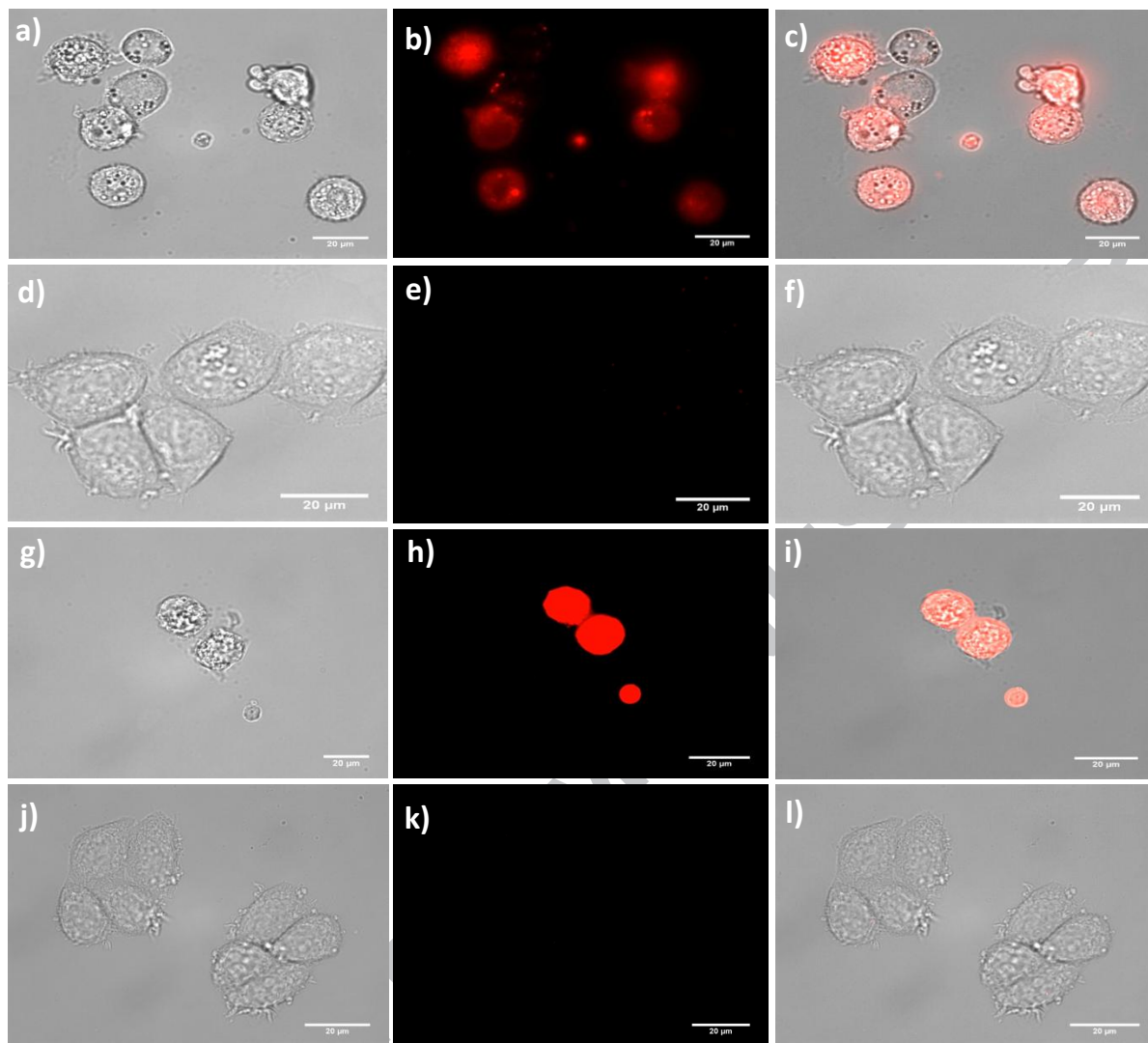


Fig. 6. Brightfield and fluorescence images of SK-BR-3 cells either incubated with $1.75 \mu\text{M}$ **Na-ZnTCPPImGNP** (a-c) and g-i)) or not incubated with nanoparticles (d-e) and j-l)) for 3 h. The cells were irradiated with a light source (400-500 nm) for 30 min and incubated for 72 h prior to imaging. Additionally, following the 72 h incubation period, propidium iodide was added to the cells to stain the nucleus of dead cells (g-l)). Images correspond to brightfield images a), d), g) and j), fluorescence images due to the fluorescence of the porphyrin on the nanoparticles b), e), h) and k), fluorescence images due to the fluorescence of the porphyrin in the **Na-ZnTCPPImGNP** together with the fluorescence from propidium iodide h) and k) and composite images of brightfield and fluorescence c), f), i) and l). The samples were excited at 530-585 nm and the fluorescence emission was collected in the red channel through a 600 nm long-pass filter. Scale bars = 20 μm .

4. Conclusions

In this work, we have successfully synthesised and characterised gold nanoparticles incorporating a tetracarboxyphenyl porphyrin linked through coordination to an imidazole connector, **Na-ZnTCPPImGNP**, and their PDT properties have been evaluated. The new approach described is elegant in its simplicity, using a stable coordinate bond, rather than the more usual covalent bonds for the incorporation of porphyrins to the gold surface.^{11,18} As far as we know, only one example of metalloporphyrins coordinated to gold nanoparticles had been reported,¹⁹ but the so-obtained nanosystem was neither water soluble nor were their PDT properties explored. HRTEM was used to characterise the morphology of GNP as well as their size. This analysis showed GNP with a cubeoctahedron shape, low polydispersity and with an average size of 8 nm. UV-visible absorption spectroscopy and HRTEM enabled the calculation of the number of molecules of porphyrin incorporated per GNP resulting in 106 molecules of **Na-ZnTCPP** per nanoparticle.

Na-ZnTCPPImGNP were able to produce singlet oxygen in a higher amount than the free porphyrin **Na-ZnTCPP** in solution, confirming previous observations for similar systems,^{12,17} a synergistic effect between gold and the immobilized photosensitizer. The maximum rate of singlet oxygen production for the free porphyrin **Na-ZnTCPP** was of 0.03%, while it increased to 0.11% when **Na-ZnTCPP** was incorporated in the **Na-ZnTCPPImGNP**. Finally, **Na-ZnTCPPImGNP** were tested *in vitro* to evaluate their PDT efficacy in SK-BR-3 human breast adenocarcinoma cells. The **Na-ZnTCPPImGNP** were internalised by the SK-BR-3 cells following an incubation period of only 3 h. Additionally, following irradiation with a blue light source of a wavelength between 400-500 nm, cell death was induced by the **Na-**

ZnTCPPImGNP. Cell death was dependent on both the concentration of the porphyrin and irradiation time, and higher phototoxicity was observed when cells were incubated with 1.75 μM of incorporated porphyrin in **Na-ZnTCPPImGNP** and irradiated for 30 min, which led to over 80% cell death using lower doses of light than the ones generally reported in the literature. Cell death was clearly visualised using fluorescence microscopy by the drastic changes in cell morphology as well as the positive staining of the cells with the cell death marker propidium iodide. The biological assays performed have demonstrated significant potential of the designed system as a theranostic agent at the boundary of optical imaging and PDT. The next step in this research may include the incorporation of targeting agents, such as antibodies, through immobilisation using the HS-C₁₁-(EG)₆-OH present on the **Na-ZnTCPPImGNP**, to specifically target cancer cells.

Disclosures

We have no conflicts of interest.

Acknowledgment

This work was supported by the EU ERDF (FEDER) funds and MINECO through Spanish Government (grant TEC2014-51940-C2-2-R). M.E.A-R thanks the *Universitat de Barcelona* for a predoctoral grant (APIF). We thank Dr D. Limón (UB) for his help with TGA analysis.

Appendix A. Supplementary material

Supplementary data associated with this article can be found, in the online version, at <http://dx.doi.org/10.1016/j.jcis.xxxx.xx.xxx>.

References

- 1 E. Alves, M. A. F. Faustino, M. G. P. M. S. Neves, Â. Cunha, H. Nadais and A. Almeida, *J. Photochem. Photobiol. C Photochem. Rev.*, 2014, **22**, 34–57.
- 2 R. Paolesse, S. Nardis, D. Monti, M. Stefanelli and C. Di Natale, *Chem. Rev.*, 2017, **117**, 2517–2583.
- 3 K. Ladomenou, M. Natali, E. Iengo, G. Charalampidis, F. Scandola and A. G. Coutsolelos, *Coord. Chem. Rev.*, 2015, **304–305**, 38–54.
- 4 L. B. Josefsen and R. W. Boyle, *Met. Based. Drugs*, 2008, 1–24.
- 5 A. Casas, G. Di Venosa, T. Hasan and Al Batlle, *Curr. Med. Chem.*, 2011, **18**, 2486–515.
- 6 U. Drechsler, B. Erdogan and V. M. Rotello, *Chem. Eur. J.*, 2004, **10**, 5570–5579.
- 7 Y. Zhou, X. Liang and Z. Dai, *Nanoscale*, 2016, **8**, 12394–12405.
- 8 C. Wang, L. Cheng and Z. Liu, *Theranostics*, 2013, **3**, 317–330.
- 9 O. Penon, T. Patiño, L. Barrios, C. Nogués, D. B. Amabilino, K. Wurst and L. Pérez-García, *ChemistryOpen*, 2015, **4**, 127–136.
- 10 M. K. K. Oo, Y. Yang, Y. Hu, M. Gomez, H. Du and Hongjun Wang, *ACS Nano*, 2012, **6**, 1939–1947.
- 11 O. Penon, M. J. Marín, D. B. Amabilino, D. A. Russell and L. Pérez-García, *J. Colloid Interface Sci.*, 2016, **462**, 154–165.
- 12 R. Lin, L. Zhou, Y. Lin, A. Wang, J. H. Zhou and S. H. Wei, *Spectroscopy*, 2011, **26**, 179–185.
- 13 A. Shinohara and H. Shinmori, *Bull. Chem. Soc. Jpn.*, 2016, **89**, 1341–1343.

- 14 J. Rochford, D. Chu, A. Hagfeldt and E. Galoppini, *J. Am. Chem. Soc.*, 2007, **129**, 4655–4665.
- 15 J. Ohyama, Y. Hitomi, Y. Higuchi, M. Shinagawa, H. Mukai, M. Kodera, K. Teramura, T. Shishido and T. Tanaka, *Chem. Commun.*, 2008, 6300–6302.
- 16 A. Kelm and J. Waluk, *Methods Appl. Fluoresc.*, 2016, **4**, 014002-014010.
- 17 O. Penon, M. J. Marín, D. A. Russell and L. Pérez-García, *J. Colloid Interface Sci.*, 2017, **496**, 100–110.
- 18 M. E. Alea-Reyes, M. Rodrigues, A. Serrà, M. Mora, M. L. Sagristá, A. González, S. Durán, M. Duch, J. A. Plaza, E. Vallés, D. A. Russell and L. Pérez-García, *RSC Adv.*, 2017, **7**, 16963–16976.
- 19 G. Fantuzzi, P. Pengo, R. Gomila, P. Ballester, C. A. Hunter, C. L. Paquato, P. Scrimin, *Chem. Commun.*, 2003, 1004–1005.
- 20 Y. Zhang, R. Yang, F. Liu and K. Li, *Anal. Chem.*, 2004, **76**, 7336–7345.
- 21 G. O. Andrés, F. M. Cabrerizo, V. Martínez-Junza and S. E. Braslavsky, *Photochem. Photobiol.*, 2007, **83**, 503–510.
- 22 M. Kanehara, H. Takahashi and T. Teranishi, *Angew. Chemie - Int. Ed.*, 2008, **47**, 307–310.
- 23 A. D. Adler, F. R. Longo, J. D. Finarelli, J. Goldmacher, J. Assour and L. Korsakoff, *J. Org. Chem.*, 1967, **32**, 476.
- 24 O. Penon, F. Marsico, D. Santucci, L. Rodríguez, D. B. Amabilino and L. Pérez-García, *J. Porphyrins Phthalocyanines*, 2012, **16**, 1293–1302.
- 25 P. E. Kolic, N. Siraj, S. Hamdan, B. P. Regmi and I. M. Warner, *J. Phys. Chem. C*, 2016, **120**, 5155–5163.

- 26 Y. Yuan, H. Lu, Z. Ji, J. Zhong, M. Ding, D. Chen, Y. Li, W. Tu, D. Cao, Z. Yu and Z. Zou, *Chem. Eng. J.*, 2015, **275**, 8–16.
- 27 M. Mojiri-Foroushani, H. Dehghani, N. Salehi-Vanani, *Electrochim. Acta*, 2013, **92**, 315–322.
- 28 F. D'Souza and O. Ito, *Chem. Commun.*, 2009, 4913–4928.
- 29 M. A Jinks, H. Sun and C. A Hunter, *Org. Biomol. Chem.*, 2014, **12**, 1440–1447.
- 30 S. V. Zaitseva, S. A. Zdanovich, A. S. Semeikin and O. I. Koifman, *Russ. J. Gen. Chem.*, 2008, **78**, 493–502.
- 31 F. D'Souza, P. M. Smith, L. Rogers, M. E. Zandler, D. M. S. Islam, Y. Araki and O. Ito, *Inorg. Chem.*, 2006, **45**, 5057–5065.
- 32 S. Wang, Y. Peng, C. Zhang, Y. Li and C. Liu, *Indian J. Chem.*, 2016, **55**, 145–152.
- 33 V. V. Apanasovich, E. G. Novikov, N. N. Yatskov, R. B. M. Koehorst, T. J. Schaafsma and A. van Hoek, *J. Appl. Spectrosc.*, 1999, **66**, 613–616.
- 34 S. J. Wang, Y. L. Peng, C. G. Zhang, Y. B. Li and C. Liu, *Bull. Korean Chem. Soc.*, 2015, **36**, 2693–2702.
- 35 G. M. Mamardashvili, O. M. Kulikova, N. V Chizhova, N. Z. Mamardashvili and O. I. Koifman, *Macroheterocycles*, 2013, **6**, 323–326.
- 36 A. Ishizaki, T. R. Calhoun, G. S. Schlau-Cohen and G. R. Fleming, *Phys. Chem. Chem. Phys.*, 2010, **12**, 7319–7337.
- 37 W. Haiss, N. T. K. Thanh, J. Aveyard and D. G. Fernig, *Anal. Chem.*, 2007, **79**, 4215–4221.
- 38 M. E. Alea-Reyes, J. Soriano, I. Mora-Espí, M. Rodrigues, D. A. Russell, L. Barrios, L. Pérez-García, *Colloids Surf. B*, 2017, **158**, 602–609.

- 39 R. Battino, T. R. Rettich and T. Tominaga, *J. Phys. Chem. Ref. Data*, 1983, **12**, 163–178.
- 40 N. Nombona, K. Maduray, E. Antunes, A. Karsten and T. Nyokong, *J. Photochem. Photobiol. B Biol.*, 2012, **107**, 35–44.
- 41 P. Schlinkert, E. Casals, M. Boyles, U. Tischler, E. Hornig, N. Tran, J. Zhao, M. Himly, M. Riediker, G. J. Oostingh, V. Puentes A. Duschl and M. Dusinska, *J. Nanobiotechnology*, 2015, **13**, 1-18.
- 42 R. Weissleder, *Nano Lett.*, 2005, **5**, 2552–2556.
- 43 K. Zaruba, J. Kralova, P. Rezanka, P. Pouckova, L. Veverkova and V. Kral, *Org. Biomol. Chem.*, 2010, **8**, 3202–3206.
- 44 B. Zhao, J. J. Yin, P. J. Bilski, C. F. Chignell, J. E. Roberts and Y. Y. He, *Toxicol. Appl. Pharmacol.*, 2009, **241**, 163–172.
- 45 T. Y. Ohulchansky, I. Roy, L. N. Goswami, Y. Chen, E. J. Bergey, R. K. Pandey, a R. Oseroff and P. N. Prasad, *Nano Lett.*, 2007, **7**, 2835–2842.
- 46 X. Liang, X. Li, L. Jing, X. Yue and Z. Dai, *Biomaterials*, 2014, **35**, 6379–6388.
- 47 A. Banerjee, P. Majumder, S. Sanyal, J. Singh, K. Jana, C. Das and D. Dasgupta, *FEBS Open Bio*, 2014, **4**, 251–259.
- 48 C. Riccardi and I. Nicoletti, *Nat. Protoc.*, 2006, **1**, 1458–1461.

